Journal of Materials Research and Technology 34 (2025) 439–448

Contents lists available at ScienceDirect

Journal of Materials Research and Technology

journal homepage: www.elsevier.com/locate/jmrt

Influence of density of a polyurethane microcellular elastomer foam on its compressive energy absorption and time-dependent behavior

Julen Cortazar-Noguerol *, Fernando Cortés, María Jesús Elejabarrieta

Department of Mechanics, Design and Industrial Management, University of Deusto, Avda. de las Universidades 24, 48007, Bilbao, Spain

ARTICLE INFO

Keywords:
Polyurethane microcellular Elastomer (PUME)
Density influence
Creep behavior
Energy absorption efficiency
Viscoelastic properties
Mechanical characterization

ABSTRACT

This study comprehensively examines the influence of density on the energy absorption capacity and the time-dependent behavior of polyurethane microcellular elastomers (PUMEs) under compression. On the one hand, to evaluate the energy absorption capacity, stress-strain curves, which can be modelled as a bilinear elastic behavior, are obtained for three different densities at two different loading rates. The data show that higher-density PUMEs exhibit greater stiffness, which is also dependent on the loading rate. Additionally, the lowest density material demonstrates the highest energy absorption efficiency at lower peak stresses and increasing the loading rate reduces efficiency across all tested densities. On the other hand, the time dependent properties are characterized through the relaxation modulus of each of the densities. To obtain it, creep experimental data is gathered and converted to relaxation through the convolution relationship between these two properties by means of Maxwell and Kelvin generalized models. The results indicate increased stiffness and longer relaxation times for higher-density PUMEs, suggesting slower responses and lower deformations under the same load. In conclusion, the increased stiffness and reduced creep compliance make higher-density PUMEs suitable for high load-bearing applications, while lower-density PUMEs are better suited for high energy absorption at lower stresses.

1. Introduction

Elastomeric foams are widely used in several fields due to their excellent energy absorption, flexibility and thermal insulation properties. These foams can dissipate impact energy through their cellular structure, which bends, twists, and buckles under stress, providing effective protection in automotive crash pads, helmets, and other safety equipment. For instance, in the automotive industry, elastomeric foams are used as viscoelastic supports for engine compartment insulation, car battery insulation, and soundproofing. They are also utilized in aerospace for impact mitigation and energy absorption in various components, enhancing safety and durability. In every mentioned application, the material works under compression.

Elastomeric foams are widely used in several fields due to their excellent energy absorption, flexibility, and thermal insulation properties [1]. Flexible polymers, in general, exhibit notable energy dissipation capabilities due to their intrinsic viscoelastic behavior, which allows them to absorb and dissipate mechanical energy through molecular chain interactions [2,3]. Polyurethane elastomers, in particular, excel in energy dissipation as their long molecular chains can stretch, slide, and reconfigure under stress, dissipating energy as heat through internal friction and molecular rearrangements [4]. By introducing a microcellular structure into polyurethane elastomers, additional energy dissipation mechanisms are enabled. These structures dissipate impact energy through the bending, twisting, and buckling of their cellular frameworks under stress, as seen in applications such as automotive crash pads, helmets, and other safety equipment [5]. For instance, in the automotive industry, elastomeric foams are used as viscoelastic supports for engine compartment insulation, car battery insulation, and soundproofing. They are also utilized in aerospace for impact mitigation and energy absorption in various components, enhancing safety and durability [6]. In all of these applications, the material primarily functions under compressive loading.

Multiple factors can affect the performance of these materials. External conditions, such as the applied preload [7] or the strain rate [8–10] must be taken into account, and usually depend on the application. Regarding the strain-rate dependence, it is a known property of viscoelastic materials and multiple studies have been performed to

* Corresponding author.
E-mail address: j.cortazar@deusto.es (J. Cortazar-Noguerol).

https://doi.org/10.1016/j.jmrt.2024.12.065
Received 1 October 2024; Received in revised form 5 December 2024; Accepted 8 December 2024
Available online 9 December 2024

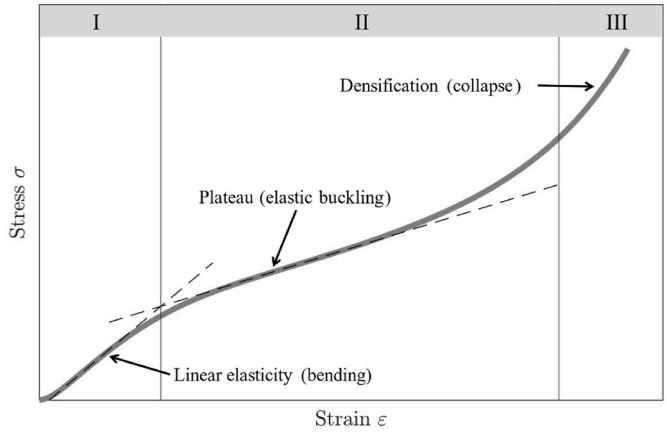

Fig. 1. Typical stress-strain curve of an elastomeric foam.

capture this behavior. In Ref. [11], Ali & Fan show the effect of the strain rate in the capabilities of a polyurethane elastomer to absorb and dissipate energy, while Cheng et al. [4] proposes a macro-mechanical model to address this effects in the same material.

In addition, the internal properties of the polyurethane elastomers, such as the microstructure [12–14] and density are known to influence the energy absorption and time-dependent properties of microcellular and nanocellular materials [15]. Regarding the effect of density, in Ref. [8], Zhao et al. study its effect on the energy absorption capabilities of an elastomeric foam. Moreover, Iqbal et al. [16] and Bhagavathula et al. [9] studied the effect of density on the compressive quasi-static response and time-dependent response of polyurethane foams respectively. In addition to density and microstructure, the incorporation of filler particles into elastomeric materials has also been studied as a method to modify their mechanical properties. For instance, hard particles can enhance stiffness and strength of elastomeric materials [17, 18].

Depending on the intended application of these materials, certain characteristics are more preferable than others. For example, in sports gears the material undergoes multiple low-velocity impacts during relatively short durations, however, shipping and packaging industry focus their needs in single impact scenarios. In contrast, for medical applications the material needs to absorb the maximum amount of energy at the minimum possible stress peak, sustaining a considerable load for long-time periods [19]. Therefore, for the selection of the optimum material internal properties (microstructure or density) both the energy absorption and the time-dependent properties need to be characterized.

On the one hand, to characterize the energy absorption behavior of an elastomeric foam at a given peak stress (or strain), the stress-strain curve can be analyzed [20,21]. In Fig. 1, a typical stress-strain curve for an elastomeric foam is shown. In this curve, three different regions can be differentiated depending on the governing mechanism of deformation. The region I is governed by the elastic bending of the cell walls resulting in a quasi-linear regime, being the slope in this region the elastic modulus of the material. The region II, known as plateau region, is associated with the beginning of the collapse of the cells. In elastomeric foams, this collapse happens by elastic buckling and is, ideally, reversible [21]. This region can also be modelled as a linear behavior, defined by the slope of the tangent curve [20]. When the cells have fully collapsed and opposing cell walls contact, the region III, called densification, begins. The densification region is characterized by a rapid increase in stress since further compressing the material implies compressing the solid itself.

On the other hand, to evaluate the time-dependent behavior of the polyurethane elastomers, the relaxation and creep properties of viscoelastic materials can be modelled using rheological models [22]. Specifically, in practical engineering applications such as the finite element modelling, to analyze the behavior of mechanical parts made of viscoelastic materials the relaxation modulus is the property from which the stiffness matrices are built [23]. However, measuring the creep compliance experimentally is a more straightforward procedure, given the usual working procedure of the experimental equipment is to exert a force and measure the displacement. Therefore, it is very important to work with models that allow the interconversion between creep and relaxation effectively.

Everything considered, the main objective of this article is to study the influence of the density in the energy absorption and time-dependent behavior in a polyurethane microcellular elastomeric (PUME) foam. These two properties have been studied on their own, both are important for material selection and this article aims to fill that gap studying both. To characterize the energy absorption, the stress-strain curves of the materials are obtained through a quasistatic and a dynamic force ramp. The time-dependent properties are obtained through creep experiments with eight different stresses. Finally, taking advantage of the convolution relationship between creep compliance and relaxation modulus, the latter is obtained through the generalized Maxwell model.

The article is organized into several sections following the introduction. First, the analytical methods to analyze the stress-strain curve are described, along with the modelling approach of the time-dependent data. Then, the materials used, the experimental setup, and the procedures for conducting stress-strain and creep experiments on PUME samples of different densities. Next, the experimental results are presented and analyzed. The following section details the modelling of the creep data and its interconversion to relaxation modulus. Finally, the

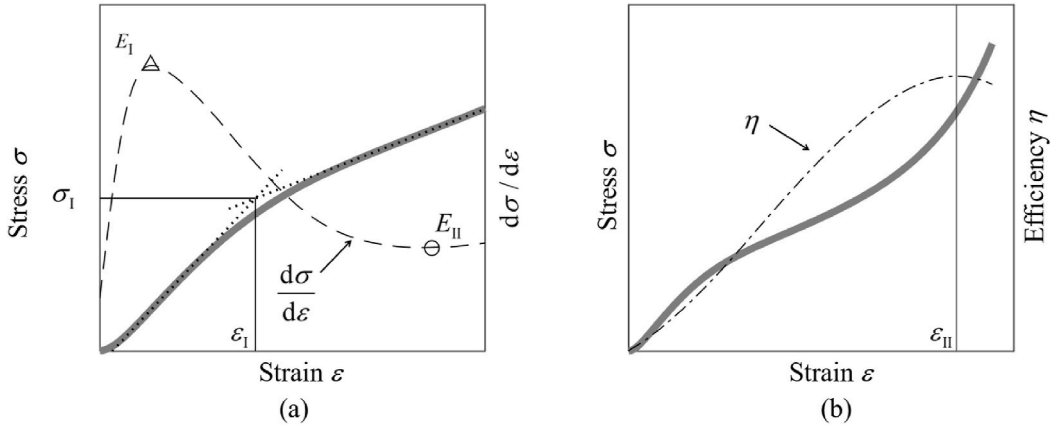

Fig. 2. Detail of the transitions of an elastomeric foam over the stress-strain curve (–): (a) plateau onset draft: stress derivative (– –) and the tangent curves of the elastic and plateau regions (···) and (b) densification onset draft: the energy absorption efficiency of the material (– · –).

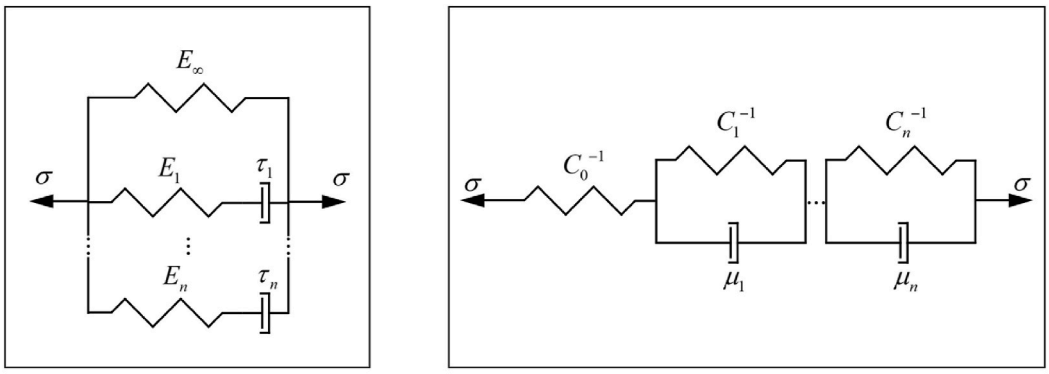

Fig. 3. Rheological model depiction of (a) the generalized Maxwell model and (b) the generalized Kelvin model.

conclusions summarize the main findings.

2. Theoretical framework

In this section, the theoretical framework is given. First, the analytic methods used to determine the span of each region of the stress-strain curve are described. Then, the generalized Maxwell and Kelvin models for the obtention of the relaxation modulus and creep compliance are presented.

2.1. Compressive stress-strain curve analysis

In this section, analytic methods for determining the span of each of the sections described are given. Specifically, in Fig. 2 the plateau and densification onsets are described in detail. The solid line represents the typical stress-strain curve. Fig. 2(a) zooms into the plateau onset, showing every parameter involved in this region transition. The dashed line represents the derivative of the stress-strain curve $\mathrm{d}\sigma/\,\mathrm{d}\varepsilon$. The derivative increases in the elastic region until its maximum E_I is reached, then, it decreases to its minimum E_II and starts to increase again after. The dotted lines in Fig. 2(a) represent the bilinear model proposed in this work. In the elastic region, the slope of the linear model is E_I and in the plateau region, the slope is E_II. In both cases, the linear model is tangent to the stress-strain curve in its inflection points. The crossing point of both tangents is the plateau onset, given by its strain ε_I and stress σ_I values and separates the elastic and plateau regions of the material represented in Fig. 1.

Fig. 2(b) shows the full span of the stress-strain curve and describes the densification onset, which can be established as the strain ε_II at which the energy absorption efficiency η is maximum and separates plateau and densification regions (see Fig. 1).The energy absorption efficiency can be defined as [10]

$$\eta(\varepsilon)=\frac{\int_0^{\varepsilon}\sigma(\varepsilon')\mathrm{d}\varepsilon'}{\sigma(\varepsilon)}=\frac{W(\varepsilon)}{\sigma(\varepsilon)}, \tag{1}$$

where $W(\varepsilon)$ represents the deformation energy absorbed up to a certain strain. The energy absorption efficiency is represented in Fig. 2(b) with a dashed-dotted line, correspondingly scaled for the sake of visualization. The energy absorption efficiency increases up to its maximum at ε_II and afterwards starts decreasing.

Concluding, from the analysis of the stress-strain curve of an elastomeric foam the deformation energy absorbed by a material can be calculated. Dividing this energy by the peak stress of the total deformation, the energy absorption efficiency is obtained. Moreover, the plateau onset and the densification onset can also be obtained, along with a bilinear model for the elastic and the plateau regions.

2.2. Modelling of time-dependent properties

In general, PUMEs exhibit a viscoelastic behavior when under static loads. This behavior can be characterized by the time-dependent strain $\varepsilon(t)$ and stress $\sigma(t)$, which are related through the relaxation modulus $E(t)$ and the creep compliance $C(t)$, according to the Boltzmann superposition principle, as follows [24]:

$$\sigma(t)=E(t)^*\dot{\varepsilon}(t)=\int_0^t E(t-\tau)\dot{\varepsilon}(\tau)\mathrm{d}\tau \tag{2}$$

and

$$\varepsilon(t)=C(t)^*\dot{\sigma}(t)=\int_0^t C(t-\tau)\dot{\sigma}(\tau)\mathrm{d}\tau, \tag{3}$$

where the * symbol represent the convolution product operator. By applying the Laplace transform to Eqs. (2) and (3) the following is obtained:

$$\widetilde{\sigma}(s)=s\widetilde{E}(s)\widetilde{\varepsilon}(s), \tag{4}$$

$$\widetilde{\varepsilon}(s)=s\widetilde{C}(s)\widetilde{\sigma}(s), \tag{5}$$

where $\widetilde{(\bullet)}(s)$ represents the Laplace transform of any $(\bullet)(t)$ function and s is the Laplace domain variable. Substituting Eq. (5) in Eq. (4):

$$\widetilde{E}(s)\widetilde{C}(s)=1/s^2, \tag{6}$$

and inversing the Laplace transform, the convolution relationship between relaxation modulus and creep compliance is obtained as

$$E(t)^*C(t)=t. \tag{7}$$

This relationship enables the interconversion between these two properties, provided an analytical model for either one is available.

Regarding modelling, one approach to model the relaxation modulus is to use the generalized Maxwell model, depicted in Fig. 3(a). When a constant strain ε_0 is applied, the resultant relaxation modulus for the generalized Maxwell model with n Maxwell elements can be described as a sum of exponential terms as [24]

$$E(t)=E_\infty+\sum_{i=1}^{n}E_i\exp\left(-\frac{t}{\tau_i}\right), \tag{8}$$

where E_∞ is the elastic modulus of the independent spring, also known as relaxed modulus, and represents the relaxation modulus when $t\to\infty$, E_i is the elastic modulus of the spring in the ith Maxwell element and τ_i is the relaxation time of the ith Maxwell element. The initial value of the relaxation modulus is $E_0=E(t=0)=E_\infty+\sum_{i=1}^{n}E_i$, which is known as the unrelaxed modulus.

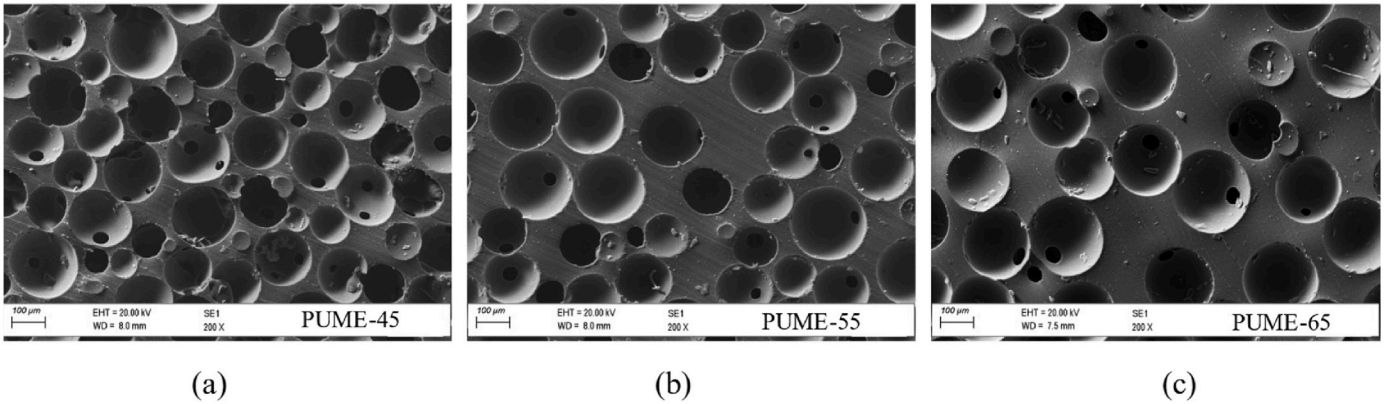

Fig. 4. SEM image of the microcellular polyurethane elastomer under study with three different densities: (a) PUME-45, (b) PUME-55 and (c) PUME-65. The image is taken with a ZEISS EVO50 microscope.

In contrast, to model the creep compliance of a viscoelastic material, the generalized Kelvin model depicted in Fig. 3(b) can be used. When a constant stress σ_0 is applied, the resultant creep compliance can be described as a sum of exponentials as follows:

$$C(t) = C_0 + \sum_{i=1}^{n} C_i \left[1 - \exp\left(-\frac{t}{\mu_i}\right)\right], \tag{9}$$

where $C_0 = C(t=0)$ is the compliance (calculated as the inverse value of the elastic modulus) of the individual spring element and represent the instantaneous creep compliance of the material, C_i is the compliance of the spring in the ith Kelvin element and μ_i is the retardation time of the ith Kelvin element. $C_\infty = C(t\to\infty) = C_0 + \sum_{i=0}^{n} C_i$ represents the long-term creep compliance.

For this work, the creep compliance is obtained experimentally and a Kelvin generalized model is fitted to the data, proving that 2 K elements ($n = 2$ in Eq. (9)) are enough to describe it. Hence, C_0, C_1, C_2, μ_1 and μ_2 are the parameters of the corresponding Kelvin model.

Making use of the convolution relationship in (7) the two term Kelvin model can be analytically transformed into a two term Maxwell model, resulting the relaxation modulus in the time domain [22]:

$$E(t) = E_\infty + E_1 \exp\left(-\frac{t}{\tau_1}\right) + E_2 \exp\left(-\frac{t}{\tau_2}\right), \tag{10}$$

where

$$E_\infty = \frac{1}{C_0 + C_1 + C_2}, \tag{11}$$

$$E_1 = E_\infty \left[\frac{C_1 + C_2}{2C_0} + \frac{\mu_1\left(C_1 - C_2 - C_2^2/C_0\right) + \mu_2\left(C_2 - C_1 - C_1^2/C_0\right)}{2\Delta^{1/2}}\right], \tag{12}$$

$$E_2 = E_\infty \left[\frac{C_1 + C_2}{2C_0} - \frac{\mu_1\left(C_1 - C_2 - C_2^2/C_0\right) + \mu_2\left(C_2 - C_1 - C_1^2/C_0\right)}{2\Delta^{1/2}}\right], \tag{13}$$

$$\tau_1 = \frac{2C_0\mu_1\mu_2}{C_0(\mu_1 + \mu_2) + C_1\mu_2 + C_2\mu_1 - \Delta^{1/2}} \tag{14}$$

and

$$\tau_2 = \frac{2C_0\mu_1\mu_2}{C_0(\mu_1 + \mu_2) + C_1\mu_2 + C_2\mu_1 + \Delta^{1/2}} \tag{15}$$

with $\Delta = (C_0\mu_1 - C_0\mu_2 - C_1\mu_2 + C_2\mu_1)^2 + 4C_1C_2\mu_1\mu_2$.

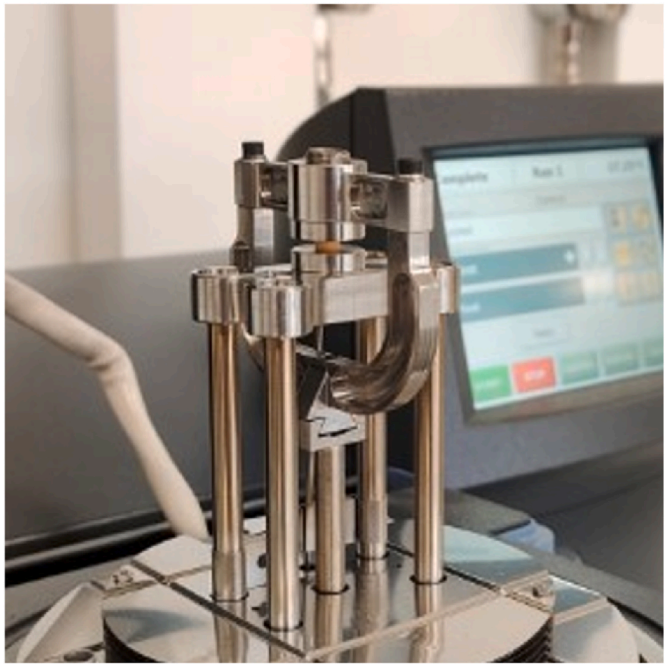

Fig. 5. Experimental configuration of the DMA compression clamp with a PUME sample.

3. Materials and methods

In this section, the material under study is described, as well as the equipment used and the experiments performed. Two different experimental methods are applied using a Dynamic Mechanical Analyzer (DMA) with a compression clamp. Initially, stress-strain curves are obtained applying two different force rates (corresponding to the quasi-static case and the maximum force rate of the equipment) in order to prove the rate dependency of the curves. Lastly, creep experimental data is gathered for eight different constant stresses.

3.1. Materials and equipment

The material studied in this work is a microcellular polyurethane elastomer. To achieve this structure, certain blowing agents are added to an isocyanate and polyol mixture (also known as polyurethane precursor). These agents release gas when exposed to heat, creating bubbles within the material, which produces the microcellular structure. Depending on the amount and composition of the blowing agents and

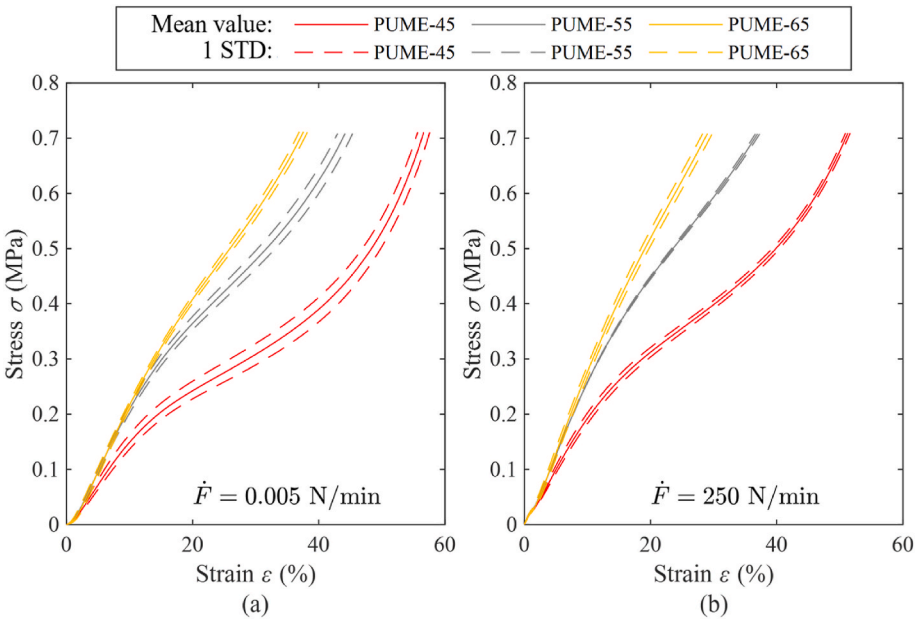

Fig. 6. Stress-strain experimental curves at different force rates: (a) quasistatic ramp and (b) fast ramp. Solid lines (–) represent the mean of three tested samples and dashed lines (– –) represent the corresponding confidence interval within one STD.

the heat and external pressure applied, different cell sizes and therefore densities can be obtained [25]. For this work, three different apparent densities are tested, namely: 450 kg/m^3, 550 kg/m^3 and 650 kg/m^3, which will be named PUME-45, PUME-55 and PUME-65 respectively throughout the rest of the article.

Fig. 4 shows a Scanning Electron Microscope (SEM) image of the three materials under study using a ZEISS EVO50 microscope. The surface of the material is treated with a 5 nm thickness Au/Pd (80:20 wt ratio) layer. In this image, the microcellular structure of the material is revealed. It can be observed that as the density increases, the pore size and shape become more uniform, and the pore distribution sparser, making, in principle, the material stiffer under compressive loads.

To ensure the repeatability of each test, three different samples are tested for every experimental procedure. The test specimens are cut using a hole puncher of 5 mm diameter from 3 mm thick material sheets.

Every test performed in this work has been done using a DMA with a compression clamp (Fig. 5), specifically, the DMA Q800 model fabricated by T.A. Instruments. This equipment can generate force-controlled displacements with range from 0.001 N to 18 N and it a rate limit of 250 N/min. The minimum sampling rate of the equipment is 10 pt/s.

3.2. Experimental methods

The stress-strain curve obtention procedure and the creep experimental procedure are described below. All experiments are performed under isothermal conditions at 35 °C. To ensure the homogeneity of the temperature within the sample, a 10-min isothermal soak is performed before every experiment.

The stress-strain curve of a material gives an overview of how the material behaves when an increasing load is applied. In viscoelastic materials, it is known that the rate at which the load is applied has an influence on their capacity to absorb deformation energy. Therefore, two different force rates $\dot{F}$ are tested. The lowest rate tested is 0.005 N/min, which is considered to be quasistatic, resulting in a 3600-min-long force ramp until the 18 N force limit of the equipment is reached with a 0.1 pt/s sampling rate. The highest rate tested is limited by the equipment at 250 N/min, resulting in a 4.32-s-long force ramp with the maximum sampling rate of the equipment (10 pt/s). From the analysis of the experimental data obtained in these experiments the values of ε_{I}, $\varepsilon_{\mathrm{II}}$, σ_{I}, E_{I} and E_{II} shown in Fig. 2 are obtained, as well as the energy absorption efficiency η of the materials.

Given the available equipment works with force-controlled displacements, the experimental obtention of the creep behavior of the material under constant stresses is straightforward. To this end, an instantaneous and constant stress is applied to the sample and the change in strain over time is measured. The tests are performed with eight different stresses and a time-span of 10 min. The selected stresses are 25 kPa, 50 kPa and from 100 kPa to 600 kPa in steps of 100 kPa. The sampling rate for these experiments is 10 pt/s. To compute the creep compliance $C(t)$ experimental values from these tests, the strain is divided by the applied stress. Once the experimental data is gathered, the parameters in Eq. (9) with $n = 2$ are optimized through a curve fitting process for each experimental curve. Then, the parameters of the relaxation modulus are obtained using Eqs. (10)–(15).

4. Stress-strain results analysis

This section presents the obtained experimental results of the force ramps. The stress-strain curves are analyzed in terms of the bilinear model proposed for the elastic and plateau regions. Next, the energy absorption properties are obtained.

4.1. Experimental results and bilinear model

The experimental results of the force ramps are shown in Fig. 6. The solid lines represent the mean result of three different samples and the dashed lines represent the confidence interval within one standard deviation (STD).

In the quasistatic curve, the three materials show an initial linear elastic region, followed by another linear elastic plateau region. At high strain, the stress starts to rapidly increase for the three materials, leading to the densification region, this increase is more pronounced in PUME-45 than in the other two densities. The PUME-65 exhibits the highest stiffness among the three materials, followed by PUME-55 and PUME-45.

For the fastest curve the behavior is similar. However, the stress values for each of the PUME is higher in this case, demonstrating the rate sensitivity of the PUME's stiffness, as expected from a viscoelastic material. In addition, the plateau region begins at lower strain and its more

Table 1
Bilinear model parameter values for the stress-strain curves.

Material	PUME-45		PUME-55		PUME-65	
$\dot{F}$ (N/min)	0.005	250	0.005	250	0.005	250
ε_I (%)	11.69	12.62	12.51	13.02	13.42	13.03
σ_I (MPa)	0.170	0.230	0.257	0.325	0.290	0.358
E_I (MPa)	1.763	2.002	2.468	2.809	2.540	3.090
E_{II}(MPa)	0.643	0.838	1.127	1.426	1.527	2.065
ε_{II} (%)	51.05	–	–	–	–	–

pronounced.

For both force rates, the PUME-65 consistently shows the stiffer response, followed by PUME-55 and PUME-45. Moreover, the difference between PUME-65 and PUME-55 is considerably lower than between PUME-55 and PUME-45, likely caused by the inhomogeneities in the microstructure shown in Fig. 4(a).

The differences in mechanical response can be further understood through the microstructural characteristics of the materials. While the polyurethane precursor used in all three densities is identical, the variations in density arise from differences in the concentration of blowing agents, leading to different pore count and distribution, as revealed in the SEM images in Fig. 4. The pore size remains relatively constant across the three densities, but lower-density PUME (PUME-45) exhibits a higher pore count and less uniform distribution. This microstructural configuration leads to thinner cell walls, resulting in lower stiffness and strength. Conversely, higher-density materials (PUME-65) feature a sparser pore distribution with greater uniformity, which enhances their ability to resist loads.

The parameters describing the plateau onset (separating the elastic and plateau regions) and the densification onset (marking the beginning on the densification region) are obtained as described in section 2.1 and shown in Table 1. It is worth to be noted that, for the stress range tested, only PUME-45 reaches densification in the quasistatic ramp and none in the fastest. From these results, a bilinear model can be built for the elastic and plateau regions. In Fig. 7, the bilinear model is superimposed to the experimental curves. The model is truncated from the densification onset onwards and the stress-strain curve in the densification region is therefore greyed out.

Based on the results in Tables 1 and it can be concluded that every parameter grows with density, except for the densification onset ε_{II}, for which there are not enough results to make any assumptions. The plateau onset strain ε_I is the less affected parameter, with less than a 20 % change between the lowest and the highest density. The plateau onset

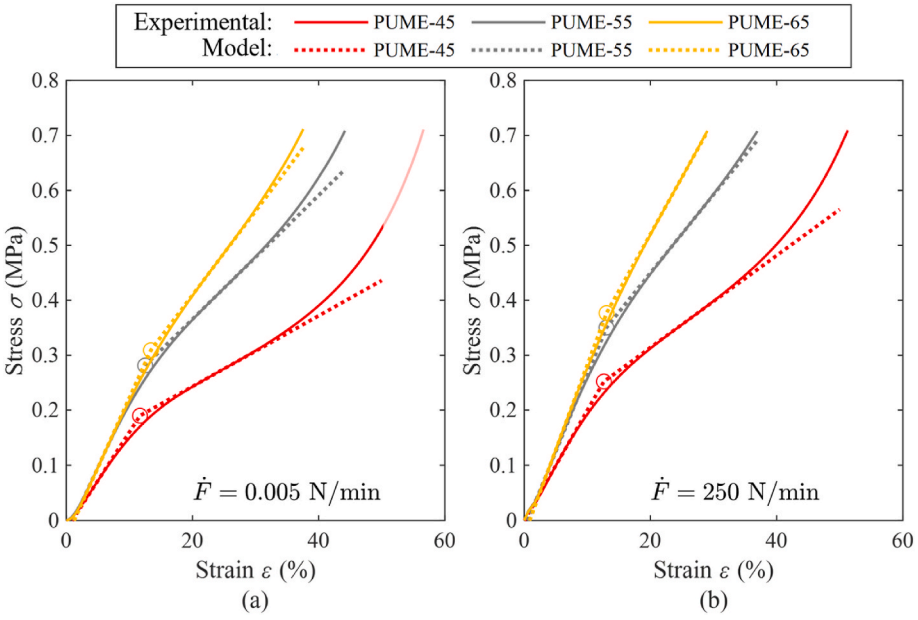

Fig. 7. Bilinear model for the stress-strain curves (–) over the experimental results (– –) for the two tested loading rates: (a) quasistatic ramp and (b) fast ramp. Circles (○) represent the plateau onset for each of the materials.

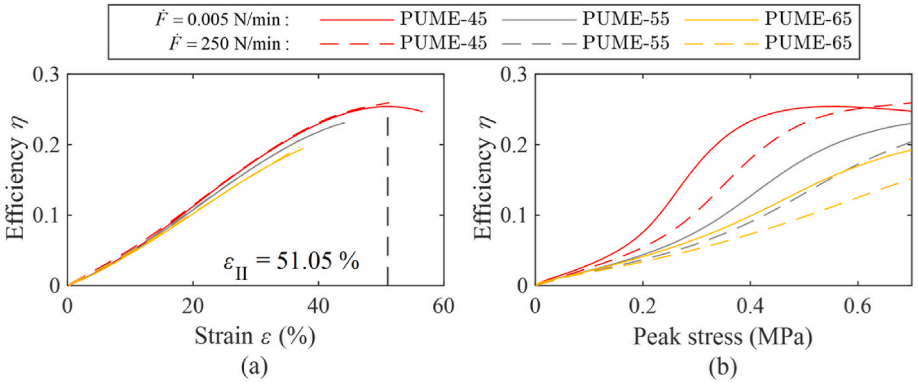

Fig. 8. Efficiency of each material as a function of (a) strain and (b) peak stress. Solid lines (–) represent the results for the quasistatic ramp (0.005 N/min) and dashed lines (– –) represent the results for the fast ramp (250 N/min).

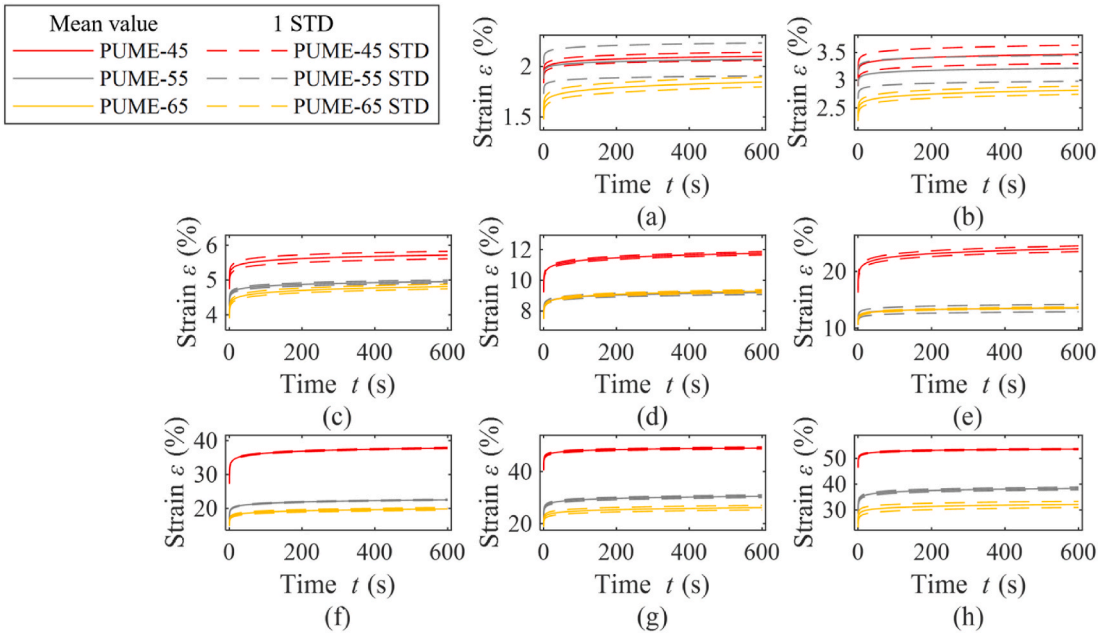

Fig. 9. Creep experiments results. The change in strain is represented for different constant loads for the three different materials. Eight different prestresses are tested: (a) 25 kPa, (b) 50 kPa, (c) 100 kPa, (d) 200 kPa, (e) 300 kPa, (f) 400 kPa, (g) 500 kPa and (h) 600 kPa. Solid lines (–) represent the mean value of the three samples and dashed lines (– –) represent the corresponding confidence interval within one standard deviation.

stress σ_I and the elastic modulus E_I show a 70 % change between the lowest and the highest density and the plateau modulus E_{II} is the most affected parameter with an increase higher than a 100 % between the lowest and the highest density. It is worth to be mentioned that the change in these parameters is not linear with density, showing a greater variation between PUME-45 and PUME-55 than between the former and PUME-65.

Regarding the dependence of the parameters with the force rate of the ramp, all of them experiment an increase in their value, except for the plateau onset strain of the PUME-65 material, which remains almost constant. Both the plateau onset stress and the plateau modulus experiment an increase of around a 30 % in their values, while the elastic modulus grows only around the 20 %. These results indicate that the bending and buckling behavior of the cell walls is influenced by the loading rate. This dependence is characteristic of viscoelastic materials and can be attributed to the inherent rate sensitivity of the elastomeric polyurethane material [4,11].

4.2. Energy absorption efficiency

To address the energy absorption capabilities of the PUMEs, Fig. 8 shows the resultant efficiency η as a function of strain and peak stress for each density. Solid lines represent the quasistatic ramp (0.005 N/min), and dashed lines represent the results for the fast ramp (250 N/min).

For both loading rates, PUME-45 demonstrated the highest efficiency, followed by PUME-55 and PUME-65 (Fig. 8(a)). PUME-45 was the only material to reach peak efficiency $\max(\eta_{45}) = 0.254$ within the tested strain range, indicating it reaches the densification region as defined in Section 2.1 for $\varepsilon_{II} = 51.05$ %. The loading rate did not significantly affect the efficiency when plotted against strain.

Similarly, when plotted against peak stress (Fig. 8(b)), PUME-45 maintains the highest efficiency across all peak stress levels for both loading rates, followed by PUME-55 and PUME-65, indicating that the lower density material is more efficient at energy absorption. For PUME-45, the efficiency grows faster for the quasi-static ramp, reaching the maximum efficiency at 554 kPa peak stress and decreasing for greater peak stresses. At 614 kPa peak stress, the efficiency of the fast ramp begins to be higher, reaching 0.259 efficiency at the limit, which is higher than the peak efficiency of the quasi-static ramp, implying that the material absorbs energy more efficiently at low deformation rates for peak stresses lower than 614 kPa, while a higher deformation rate is preferred for higher peak stresses.

In the stress range tested, PUME-55 and PUME-65 show a similar behavior. PUME-55 shows a higher energy absorption efficiency in the whole range, being the lower deformation rate more efficient. PUME-65 shows the lowest energy absorption efficiency of the three materials tested, being the lower deformation rate more efficient.

These results highlight the significant impact of density and loading rate on the mechanical behavior of PUMEs, with higher density materials being more suitable for applications requiring greater load-bearing capacity and stiffness. However, for applications requiring a high energy absorption at low peak stresses, lower density materials perform better.

5. Relaxation model development

In this section, the results regarding the creep experiments are shown, along with the curve fitting of the Kelvin model and the consequent obtention of the Maxwell relaxation model.

5.1. Creep experimental results

Fig. 9 shows the creep experimental results of the three tested densities. The solid lines represent the mean value of four different samples and the dashed lines represent the corresponding confidence interval within one standard deviation. The experimental results show that up to 50 kPa the three different densities behave similarly. From 100 kPa onwards, the PUME-45 starts to deviate from the rest, with a significant increase in strain, while the PUME-55 and PUME-65 curves overlap. From 400 kPa onwards the strain in the PUME-55 samples start to be noticeably bigger than that from the PUME-65 samples.

The creep experiments demonstrate that the strain response of PUMEs is significantly influenced by both material density and the level of applied stress. PUME-65 is more resistant to creep, exhibiting lower strain under constant load, whereas PUME-45 is more prone to deformation.

Table 2
Last evaluation of the objective function in the curve fitting process.

Material	MSE	R^2
PUME-45	2.66×10^{-6}	0.9902
PUME-55	1.37×10^{-6}	0.9899
PUME-65	1.45×10^{-6}	0.9909

5.2. Maxwell model development

In this section, the two term Kelvin model parameters described in Section 2.2 will be fitted to the creep experimental results. Then, by using the convolution product relationship described in Section 2.2, the Maxwell model for the relaxation modulus is developed. To obtain the creep compliance $C(t)$ from the experimental results in Fig. 9, the strain ε is divided by the applied stress σ_0.

For the curve fitting process, Matlab's *'fmincon'* (MATLAB 2023a) function has been used. The mean squared error (MSE) between the experimental data and analytical function in Eq. (9) is used as objective function:

$$\mathrm{MSE} = \frac{1}{m}\sum_{j=1}^{m}\frac{1}{N}\sum_{i=1}^{N}\left[C_{\exp}(t_i,\sigma_j) - C_{\mathrm{K}}(t_i,\sigma_j)\right]^2, \tag{16}$$

where m is the total number of stresses tested, N is the total number of time-steps $C_{\exp}(t_i,\sigma_j)$ and $C_{\mathrm{K}}(t_i,\sigma_j)$ are the experimental and Kelvin model creep compliances respectively, as a function of time t_i and stress applied σ_i.

As shown in Eq. (9), the model has 5 independent parameters, whose values are optimized to minimize the objective function. In Table 2, the last evaluation of the objective function and the coefficient of determination R^2 is shown. Based on the values of R^2, the curve fitting process is successful and the model correctly represents the experimental data.

Fig. 10 illustrates the fitting parameters from the generalized Kelvin model for the creep behavior of PUMEs with different densities for the whole tested stress range. The initial creep compliance C_0 and the long-term creep compliance C_∞ show a similar behavior. Both exhibit a decreasing tendency at low stresses, continued by an increase. In the case of PUME-45, the tendency becomes decreasing again when the densification onset is reached. In both cases, PUME-45 shows a greater compliance, followed by PUME-55 and PUME-65, demonstrating that greater densities lead to stiffer materials, less prone to deformation.

Retardation times μ_1 and μ_2 decrease with increasing stress for all materials. Although the differences are not extreme, PUME-65 shows higher retardation times than the rest of the materials. PUME-55 and PUME-45 show a similar behavior up until 300 kPa and deviate from 400 kPa onwards. PUME-45 is the material with the lowest retardation times, indicating a faster response than the rest of the materials.

Using Eqs. (11)–(15), the relaxation modulus parameters for the generalized Maxwell model (10) can be obtained from the values represented in Fig. 10. Given the generalized Maxwell model is developed for constant strains, a transformation from the stress σ_0 to the strain ε_0 independent variable is needed. In this regard, it must be noted that for long-time periods, where $t \to \infty$,

$$E_\infty = \sigma(t\to\infty)/\varepsilon_0 \tag{17}$$

and

$$C_\infty = \varepsilon(t\to\infty)/\sigma_0. \tag{18}$$

Hence, Eq. (11) proves that $E_\infty = C_\infty^{-1}$. Therefore, σ_0 and ε_0 can be related by

$$\varepsilon_0 = C_\infty \sigma_0. \tag{19}$$

Using Eq. (19), in Fig. 11 the evolution of the Maxwell model parameters with strain for each of the material densities is presented. As expected, this figure shows a behavior complementary to Fig. 10.

The initial E_0 and long-term E_∞ modulus have a similar behavior and

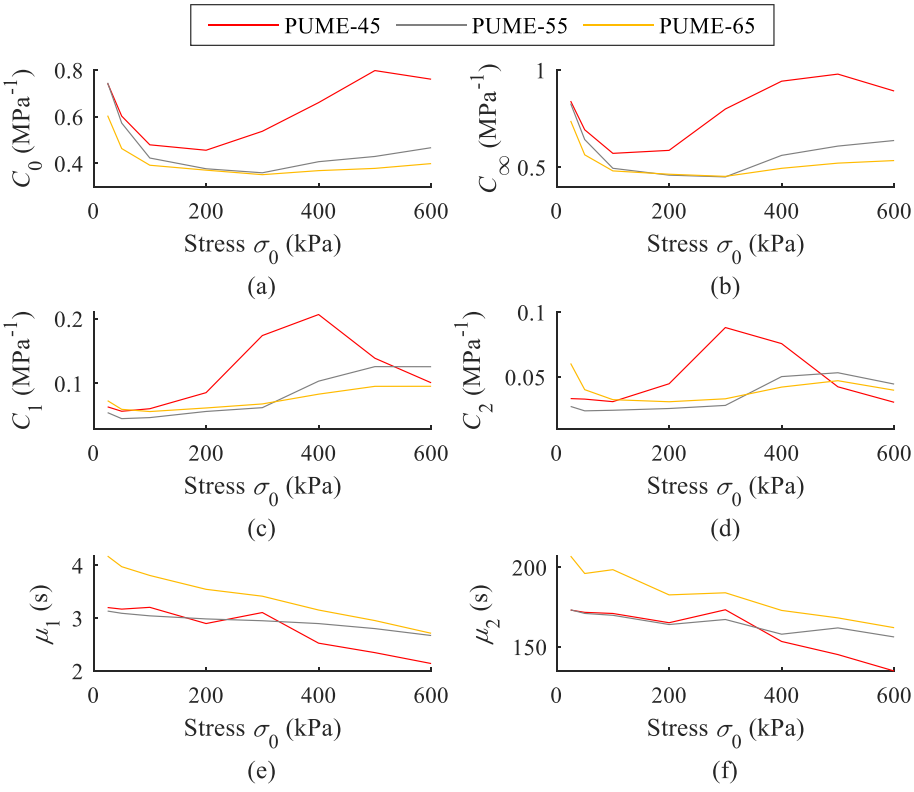

Fig. 10. Obtained results for each of the parameters of the creep generalized Kelvin model as a function of stress after the curve fitting process: (a) C_0, (b) $C_\infty = C_0 + C_1 + C_2$, (c) C_1, (d) C_2, (e) μ_1 and (f) μ_2.

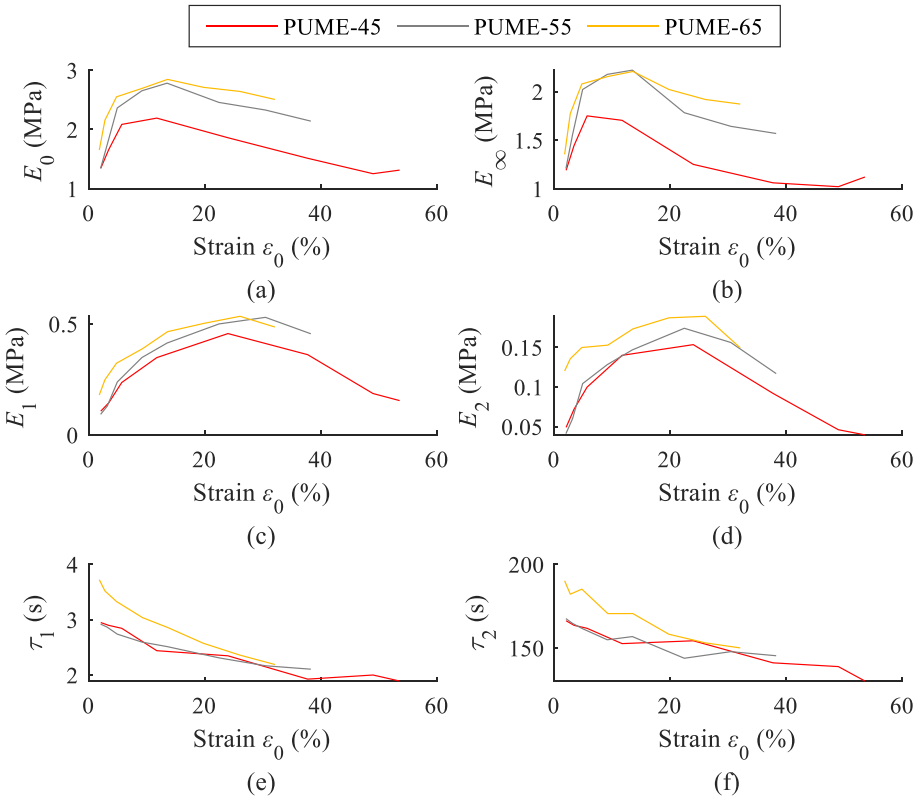

Fig. 11. Obtained results for each of the parameters of the relaxation generalized Maxwell model as a function of strain. (a) $E_0 = E_\infty + E_1 + E_2$, (b) E_∞, (c) E_1, (d) E_2, (e) τ_1 and (f) τ_2.

opposite to what the initial and long-term creep compliances showed. In contrast, the relaxation times τ_1 and τ_2 show a slightly lower values than the retardation times, but with the same decreasing tendency when higher strains are applied. Moreover, the PUME-65 retardation time shows a higher value for low strains and tends to similar values of PUME-55 and PUME-45 when greater strains are applied.

6. Conclusions

This study comprehensively examined the mechanical behavior of PUME foams, providing valuable insights into the influence of material density on energy absorption efficiency and long-term behavior.

The experimental stress-strain results demonstrate that higher density PUMEs have greater stiffness. The proposed bilinear model allowed for the elastic and plateau region characterization, showing an increasing plateau onset stress for higher densities (70 % increase) while the strain is much less affected (15 % increase). Only PUME-45 reaches the densification onset in the quasistatic ramp at 51.05 % strain. Based on the same curves, the energy absorption efficiency can also be evaluated. In the range tested, PUME-45 shows the greatest energy absorption efficiency, reaching its global maximum (0.254) at 554 kPa. PUME-55 and PUME-65 show an increasing tendency, but do not reach a maximum.

Regarding the fast ramps, the material shows an increase of 30 % in the plateau onset stress and the plateau modulus and 20 % increase in the elastic modulus, while the plateau onset strain remains almost constant for the three densities. Energy absorption efficiency remains unaffected by the loading rate when plotted against strain, although it shows an increase in peak stress for the same energy absorption efficiency levels for the three tested densities.

The generalized Kelvin model effectively captures and help in the description of the creep behavior of PUMEs. PUME-65 shows a lower creep overall with higher retardation times, indicating lower deformations and slower responses for higher densities under the same load. Retardation time also decreases with the applied stress, showing faster responses for increasing loads. The derived relaxation modulus corroborates the previous findings but show lower relaxation times, indicating the relaxation phenomena occurs faster than the creep.

The increased stiffness and reduced creep compliance make higher density PUMEs more suitable for applications requiring higher load-bearing capacity. Conversely, lower density PUMEs, with their higher energy absorption efficiency, are better suited for applications needing high energy absorption at lower stresses.

Declaration of competing interest

The authors declare that they have no known competing financial interests or personal relationships that could have appeared to influence the work reported in this paper.

Acknowledgements

This study received financial support from Orona EIC S. Coop., from the Department of Education for the Research Group program IT1507–22 and Department of Economic Development, Sustainability and Environment project KK-2022/00050 of Basque Government.

References

[1] Rostami-Tapeh-Esmaeil E, Vahidifar A, Esmizadeh E, Rodrigue D. Chemistry, processing, properties, and applications of rubber foams. Polymers 2021;13:1565. https://doi.org/10.3390/polym13101565.

[2] Fan JT, Weerheijm J, Sluys LJ. Dynamic compressive mechanical response of a soft polymer material. Mater Des 2015;79:73–85. https://doi.org/10.1016/j.matdes.2015.04.035.

[3] Fan J, Wang C. Dynamic compressive response of a developed polymer composite at different strain rates. Compos Part B Eng 2018;152:96–101. https://doi.org/10.1016/j.compositesb.2018.06.025.

[4] Fateh Ali S, Fan J, Feng J, Wei X. A macro-mechanical study for capturing the dynamic behaviors of a rate-dependent elastomer and clarifying the energy dissipation mechanisms at various strain rates. Acta Mech Solida Sin 2022;35:228–38. https://doi.org/10.1007/s10338-021-00263-7.
[5] Koohbor B, Youssef G, Uddin KZ, Kokash Y. Dynamic behavior and impact tolerance of elastomeric foams subjected to multiple impact conditions. J Dyn Behav Mater 2022;8:359–70. https://doi.org/10.1007/s40870-022-00340-z.
[6] Elastomeric foams. ISOVER St-GOBAIN n.d. https://www.isover-technical-insulation.com/elastomeric-foams (accessed July 3, 2024).
[7] Cortazar-Noguerol J, Cortés F, Sarría I, Elejabarrieta MJ. Preload influence on the dynamic properties of a polyurethane elastomeric foam. Polymers 2024;16:1844. https://doi.org/10.3390/polym16131844.
[8] Zhao Z, Li X, Jiang H, Su X, Zhang X, Zou M. Study on the mechanical properties and energy absorbing capability of polyurethane microcellular elastomers under different compressive strain rates. Polymers 2023;15:778. https://doi.org/10.3390/polym15030778.
[9] Bhagavathula KB, Meredith CS, Ouellet S, Satapathy SS, Romanyk DL, Hogan JD. Density, microstructure, and strain-rate effects on the compressive response of polyurethane foams. Exp Mech 2022;62:505–19. https://doi.org/10.1007/s11340-021-00772-z.
[10] Li QM, Magkiriadis I, Harrigan JJ. Compressive strain at the onset of densification of cellular solids. J Cell Plast 2006;42:371–92. https://doi.org/10.1177/0021955X06063519.
[11] Ali SF, Fan J. Capturing dynamic behaviors of a rate sensitive, elastomer with strain energy absorptions and dissipation effects. Int J Appl Mech 2021;13:2150104. https://doi.org/10.1142/S1758825121501040.
[12] Wu Y, Lu S, Zhang C, Wang C, Fang H. Unveiling the three-dimensional network and deformation mechanism of foamed polyurethane by coarse-grained and graph theory. J Mater Res Technol 2024;29:4650–61. https://doi.org/10.1016/j.jmrt.2024.02.156.
[13] Gao J, Hu F, Yang H, Qi F, Zhao N, Zhang B, et al. Study on mechanical behaviors and failure mechanism of polyurethane matrix composites inspired by mussel chemistry and arthropod exoskeleton structures under dynamic impact. J Mater Res Technol 2023;25:2227–39. https://doi.org/10.1016/j.jmrt.2023.06.028.
[14] Naveen Kumar G, Rajesh K, Rama Durga Rao M, Sai Bharath KP, Eswara Manikanta J. A review on mechanical properties of hybrid polymer composites. Mater Today Proc 2023. https://doi.org/10.1016/j.matpr.2023.05.059.
[15] Le Barbenchon L, Kopp J-B. A review on the mechanical behaviour of microcellular and nanocellular polymeric foams: what is the effect of the cell size reduction? J Cell Plast 2024:0021955X241246066. https://doi.org/10.1177/0021955X241246066.
[16] Iqbal N, Mubashar A, Ahmed S, Arif N, Din E-U. Investigating relative density effects on quasi-static response of high-density Rigid Polyurethane Foam (RPUF). Mater Today Commun 2022;31:103320. https://doi.org/10.1016/j.mtcomm.2022.103320.
[17] Fan JT, Weerheijm J, Sluys LJ. Glass interface effect on high-strain-rate tensile response of a soft polyurethane elastomeric polymer material. Compos Sci Technol 2015;118:55–62. https://doi.org/10.1016/j.compscitech.2015.08.007.
[18] Fan JT, Weerheijm J, Sluys LJ. Compressive response of a glass–polymer system at various strain rates. Mech Mater 2016;95:49–59. https://doi.org/10.1016/j.mechmat.2015.12.005.
[19] Abdullah M, Ramtani S, Yagoubi N. Mechanical properties of polyurethane foam for potential application in the prevention and treatment of pressure ulcers. Results Eng 2023;19:101237. https://doi.org/10.1016/j.rineng.2023.101237.
[20] Albuquerque RQ, Meuchelböck J, Ruckdäschel H. A unified approach for evaluating mechanical compression tests for polymer bead foams. J Polym Sci 2023:20230704. https://doi.org/10.1002/pol.20230704. pol.
[21] Gibson LJ, Ashby MF. Cellular solids: structure and properties. With corrections. second ed. Cambridge: CUP; 1999.
[22] Luo R, Lv H, Liu H. Development of Prony series models based on continuous relaxation spectrums for relaxation moduli determined using creep tests. Constr Build Mater 2018;168:758–70. https://doi.org/10.1016/j.conbuildmat.2018.02.036.
[23] Wang X, Wang Y, Qiang H, Bai J, Luo C, Zhao Z. Initial stress approach-based finite element analysis for viscoelastic materials under generalized Maxwell model. AIP Adv 2024;14:065132. https://doi.org/10.1063/5.0204292.
[24] Altenbach H, Öchsner A. Encyclopedia of continuum mechanics. Berlin, Heidelberg: Springer; 2020.
[25] Reghunadhan A, Thomas S. Polyurethanes. Polyurethane polym. Elsevier; 2017. p. 1–16. https://doi.org/10.1016/B978-0-12-804039-3.00001-4.